Available online at www.sciencedirect.com

ScienceDirect

Advances in Space Research 71 (2023) 2691–2701

ADVANCES IN SPACE RESEARCH (a COSPAR publication)

www.elsevier.com/locate/asr

System-level prognostics approach for failure prediction of reaction wheel motor in satellites

Hyung Jun Park [a,1], Seokgoo Kim [b,1], Junyoung Lee [c], Nam Ho Kim [b], Joo-Ho Choi [d,*]

[a] Dept. of Smart Air Mobility, Korea Aerospace University, Gyeong gi-do 10540, Republic of Korea
[b] Dept. of Mechanical and Aerospace Engineering, University of Florida, Gainesville 32611, USA
[c] Dept. of Aerospace and Mechanical Engineering, Korea Aerospace University, Gyeong gi-do 10540, Republic of Korea
[d] School. of Aerospace and Mechanical Engineering, Korea Aerospace University, Gyeong gi-do 10540, Republic of Korea

Received 29 June 2022; received in revised form 9 November 2022; accepted 14 November 2022
Available online 21 November 2022

Abstract

The reaction wheels actuated by motors are widely used for advanced attitude control of satellites. During the satellite operation, the performance of reaction wheel motor degrades and results in unexpected failures. To guarantee the reliability and safety of satellites, it is important to predict its remaining useful life while it is in operation. To address this issue, this study presents a system-level prognostics approach for the reaction wheel motor, by regarding it as a system composed of multiple components. The approach is demonstrated by using the motor operation data obtained during the accelerated-life tests on ground for 3 years. Health degradation of each components of the motor are estimated using the adaptive extended Kalman filter. Failure threshold of the motor performance is established by the design requirement on characteristic curve. The anomaly detection and failure prediction are performed using the shifting kernel particle filter.
© 2022 COSPAR. Published by Elsevier B.V. All rights reserved.

Keywords: Accelerated life test; Extended Kalman filter; Particle filter; Prognostics; Reaction wheel motor; Satellite

1. Introduction

Satellites in space require accurate attitude control and high reliability to fully conduct their mission. The reaction wheel (RW) actuated by a motor provides consistent angular momentum to help stabilize satellite from external torques such as solar radiation pressure and to control its precise attitude as illustrated in Fig. 1. However, the function of the motor degrades by continuous operation and eventually impacts the reliability of the whole satellite control system (Hu et al., 2012). According to the survey on the failure statistics of satellite components, most failures are attributed to the actuators of attitude and control system (AOCS) such as RW motor (Ji et al., 2019). Therefore, the methods to monitor health and predict degradation of RW motor are necessary to achieve such reliability.

Recently, several publications have been conducted on the health management of satellite components, emphasizing its importance in spacecraft operation service, which can be divided into fault diagnosis and failure prognosis. In the fault diagnosis, Tudoroiu et al. (2006) developed interacting multiple models Unscented Kalman filter (IMM-UKF) to detect various fault modes in the RWs including unexpected changes in power supply bus voltage and motor current variations. Rahimi et al. (2017) used adaptive UKF (AUKF) to detect abrupt and intermittent faults in the RW and control moment gyros (CMG). In a more recent effort, Rahimi et al. (2020a) addressed a new

* Corresponding author.
E-mail address: jhchoi@kau.ac.kr (J.-H. Choi).
[1] Hyung Jun Park and Seokgoo Kim are co-first authors.

https://doi.org/10.1016/j.asr.2022.11.028
0273-1177/© 2022 COSPAR. Published by Elsevier B.V. All rights reserved.

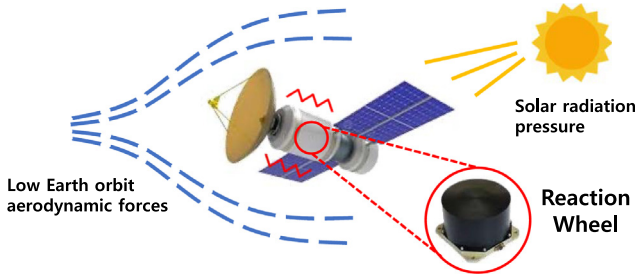

Fig. 1. External torques to satellite in space.

hierarchical method for fault diagnosis for RW faults which used the residual signals with an adaptive threshold technique. A dual unscented Kalman filter is used for fault identification by states and parameter estimation. Aghalari and Shahravi (2017) proposed improved electro-mechanical modeling of RW for more robust fault estimation and isolation. While the above studies are based on the model-based approaches, others have addressed the data-driven approaches which highly depend on the quality and quantity of the measured data. Muthusamy and Kumar (2021) proposed a fault detection scheme for motor faults in satellite control systems using Chebyshev Neural Network. Rahimi and Saadat (2020) applied an ensemble machine-learning method with various classifiers to detect faults in the RW motor current and bus voltage. Nozari et al. (2019) proposed multiple classifier-based fault detection schemes with four classification algorithms to deal with the combined simultaneous faults. Abd-Elhay et al. (2022) proposed a deep learning architecture that combined a one-dimensional Convolutional Neural Network (1D-CNN) and Long Short-Term Memory (LSTM) to detect and identify RW fault modes such as motor current loss and high friction. Lee et al. (2020) also applied the deep learning method using the residuals between the measured attitude data and the estimated attitude data and verified its performance based on simulation.

However, unlike the motors on ground, fault diagnosis in space is of less importance since the immediate maintenance or replacement is impossible for the space system. Instead, the failure prognosis that predicts remaining useful life (RUL) is more useful as a means to ensure the safe operation period in space and to aid decision making as early as possible. The RUL prediction can provide the time for engineers on the ground to prepare and counteract the upcoming satellite failure.

Few studies are found for the prognostics in the satellite applications, in which most articles are focused on the Li-ion battery for satellite electrical power (Cao et al., 2019; Jun et al., 2012; Liu et al., 2013; Song et al., 2017; Zhang et al., 2018). Only few papers have addressed the prognostics of RW motor. Wang et al. (2016) explored data-driven approach to predict the bearing life in the RW using a neural network (NN) algorithm. They have considered bearing temperature and rotating speed as the health indicators (HI) and the NN is trained with historical HIs to predict the future RUL. Muthusamy and Kumar (2022) proposed General path model and Bayesian updating technique to predict failure of spin motor in the control moment gyros (CMGs) using attitude measurement data. Rahimi et al. (2020b) have taken model-based approach by applying adaptive Unscented Kalman filter (UKF) to estimate the parameter related to the bearing friction change and predict RUL until failure using Particle filter (PF). However, there are several limitations in these papers. First, the studies are conducted using the simulated run-to-failure data generated by the model, which can differ from actual degradation and need additional validation with an actual degradation process. Second, the failure threshold is set arbitrary which lacks physical ground and may lead to the wrong RUL. Third, while the motor is regarded as a single component, it is also a system in itself since it consists of electrical and mechanical components with multiple failure modes. Since each component's degradation affect the motor performance, the RUL should be predicted accounting for this, which we call the system-level prognostics.

Motivated by the above limitations and requirements, this paper addresses the RUL prediction of RW motor based on the system-level prognostics architecture. The architecture was recently proposed by the authors (Kim et al., 2021), in which the motor was taken to demonstrate the procedure, but it was conducted by the virtual data made by the model dynamics. The main idea is based on the fact that if any system degrades in performance, it is due to those of the underlying components. In this study, we have conducted accelerated-life test (ALT) on the RW motor for the period of 3 years to acquire real measurement data with the low sampling rate, same as the space environment. A proper failure threshold is imposed on the motor based on the characteristic curve given by the design requirement. The RUL is predicted using the degradation relation between the system and components, assuming the data as being obtained during the space operation.

The rest of the article is organized as follows. Section 2 explains an experimental setup for ALT and the measurement process. In Section 3, the on-line diagnosis and off-line prognosis part of the framework is address with the used algorithms. In additional, application to ALT data is explained. In Section 4, the application result is represented and Section 5 concludes this article.

2. Experimental setup

The RW in this study is developed for the Korean Space Launch Vehicle, of which the name is Science and Technology Satellite-3 (STSAT-3), and addressed in (Kim et al., 2010). It is actuated by the motor to provide consistent angular momentum and control its precise attitude. The motor specification is described in Table 1. For this motor, the ALT is performed, in which a cycle consists of the operation with a short-term pull-up and a long-term constant speed as shown in Fig. 2. During the operation, the current

Table 1
Motor specification.

SRB-361-1103 Motor	
Diameter	139 mm
Height	51.5 mm
Total mass	1.38 kg
Wheel inertia	0.001143 kgm^2
Torque constant	0.0568 Nm/A
Friction coefficient (bearing)	1.01 $\times 10^{-5}$
Friction coefficient (air drag)	0.72 $\times 10^{-5}$
Current	(24 V)
Steady state @ 3000 rpm	0.19A

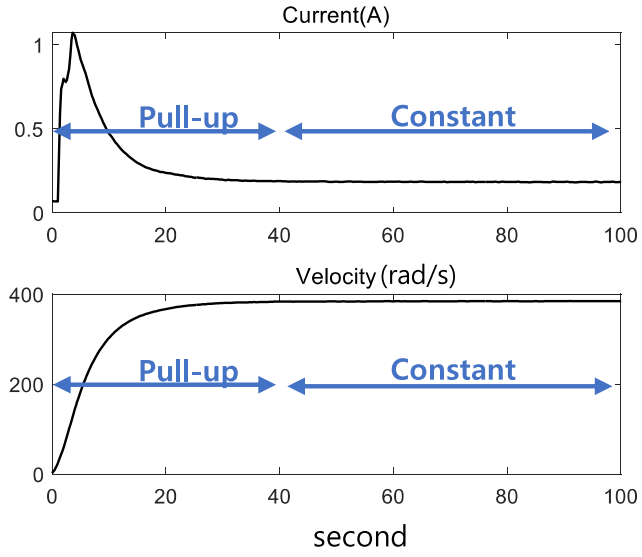

Fig. 2. Measured current and angular velocity signal in a cycle.

and angular velocity signals are acquired at a 2 Hz sampling rate. The pull-up test lasts only for few seconds, while the rest of the time is given for the constant speed test, which takes from 10 to 20 h. As a result, a day is spent in average for a single cycle operation, and the whole test lasts for 3 years. The pull-up operation is to evaluate the motor performance by applying a maximum voltage to the motor. The test is conducted under two extreme temperature conditions: hot (60 °C) and cold (−30 °C) temperature in the thermal vacuum chamber to evaluate its reliability and performance. Despite the long period of 3 years, the test did not reach failure, and is stopped because of the abnormal high current consumption and safety issues.

3. Methodology

The overall framework of the system-level prognosis is illustrated in Fig. 3. It consists of two stages: on-line diagnosis and prediction at the upper part, and off-line monitoring and prognosis at the lower part. In the on-line diagnosis, the state and measurement models are developed based on the electro-mechanical dynamic model. Then the health parameters denoted by k_T and b are estimated for a cycle by the Adaptive Extended Kalman Filter (AEKF) (Wang et al., 2021; Zhou et al., 2010) using the acquired motor operation data ω and i. Once the health parameters are estimated, system performance is evaluated, which is defined by the torque $J\dot{\omega}$ at a certain velocity ω^* as shown on the upper right in Fig. 3. In the lower part, namely the off-line monitoring and prognosis, the estimated health parameters from each cycle are exploited to monitor the degradation trend over long-term cycles and to predict their future behavior as shown on the left. The Shifting Kernel Particle Filter (SKPF) algorithm is used for this purpose (Kim et al., 2020), in which the anomaly from normal state is detected and its degradation is predicted in a single frame. Then the predicted health parameters are transferred to the upper part, i.e., the on-line prediction to predict the system performance in the future. Finally, the end of life (EOL) of system performance is obtained against a threshold given by the design requirement. Further details are addressed in the following subsections.

3.1. On-line parameter estimation

In the on-line diagnosis, the Extended Kalman Filter (EKF) is used to estimate the health state based on the motor dynamic model and measured signals from each cycle. While the detail of the EKF for motor system can be found in (Bavdekar et al., 2011; Singleton et al., 2015), they are summarized here for brevity. The governing equations of the mechanical and electrical part of the motor are given by:

$$\begin{aligned} &\text{Mechanical part } J\tfrac{d\omega}{dt} + b\omega = k_T i - T_L \\ &\text{Electrical part } L\tfrac{di}{dt} + Ri = V - k_T\omega \end{aligned} \tag{1}$$

where V is the input voltage and ω and i are the angular velocity and current, which are the output state variable to be obtained as the solution. Table 2 explains the model parameters used in this study. Among these, the health parameters responsible for the motor performance degradation are given by $\boldsymbol{h} = [k_T, b]^T$ which are the back EMF coefficient and the friction coefficient. They are related with the bearing and permanent magnet health, respectively. To apply the EKF to this model, the state and measurement model are formulated from (1), which are

$$\boldsymbol{x} = \begin{bmatrix} \dot{\omega} \\ \dot{i} \end{bmatrix} = \begin{bmatrix} -\frac{b}{J} & \frac{k_T}{J} \\ -\frac{k_T}{L} & -\frac{R}{L} \end{bmatrix} \begin{bmatrix} \omega \\ i \end{bmatrix} + \begin{bmatrix} -\frac{T_L}{J} \\ \frac{V}{L} \end{bmatrix} \tag{2}$$

$$\boldsymbol{z} = \begin{bmatrix} 1 & 0 \\ 0 & 1 \end{bmatrix} \begin{bmatrix} \omega \\ i \end{bmatrix} + \boldsymbol{v} \tag{3}$$

where equation (2) is the recursive expression of (1), in which $\boldsymbol{x} = [\omega, i]^T$ represents the state variable to be determined by the EKF. Equation (3) is the measurement model, in which $\mathbf{z}$ represents the measurement of state variable $\boldsymbol{x}$ and $\boldsymbol{v}$ is the associated noise. In the EKF, the state and measurement model are further transformed to the discrete form for the estimation, in which the state variable is augmented by the health parameters $\boldsymbol{h}$, i.e., the state vari-

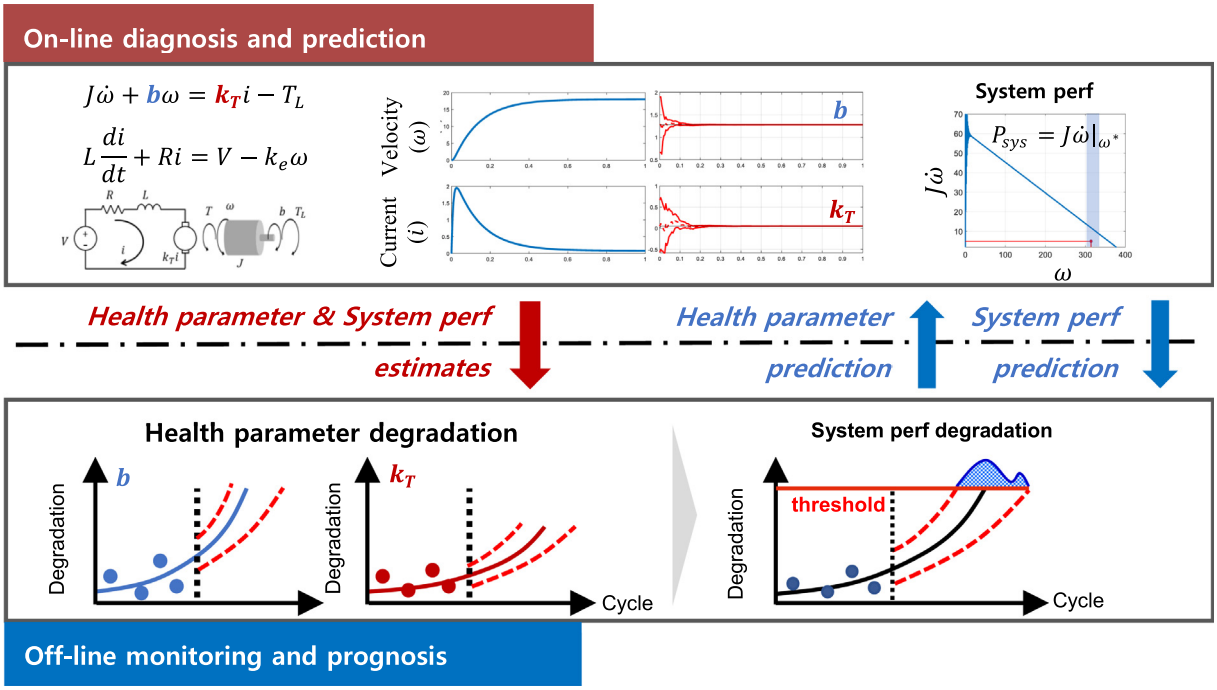

Fig. 3. Framework of the proposed method (Kim et al., 2021).

Table 2
Parameter description and values for EKF.

Symbol	Description	Value
R	Armature resistance	22 Ω
L	Armature inductance	0.1215 H
J	Moment of inertia	0.001143 kg m^2
b	Friction coefficient	1.01×10^{-5} N m s/rad
k_T	Electro-mechanical coupling coefficient	0.054 Nm/A
V	Input voltage	24 V
T_L	Load torque	0.0001 Nm

able vector $\boldsymbol{x_t}$ includes the original state variable $\boldsymbol{x}$ and health parameter $\boldsymbol{h}$. They are given by:

State model: $\boldsymbol{x_t} = F(\boldsymbol{x_{t-1}}, u_{t-1}) + \boldsymbol{w}_{t-1}$ or

$$\begin{bmatrix} \omega_t \\ i_t \\ k_{T,t} \\ b_t \end{bmatrix} = \begin{bmatrix} \left(1 - b_{t-1}\frac{dt}{J}\right)\omega_{t-1} + \frac{dt}{J}\left(k_{T,t-1}i_{t-1} - T_L\right) \\ -k_{T,t-1}\cdot\omega_{t-1}\cdot\frac{dt}{L} + \left(1 - R\cdot\frac{dt}{L}\right)i_{t-1} + V\cdot\frac{dt}{L} \\ k_{T,t-1} \\ b_{t-1} \end{bmatrix} + \boldsymbol{w}_{t-1} \tag{4}$$

Measurement: $\boldsymbol{z_t} = H(\boldsymbol{x_t}) + \boldsymbol{v}_t$ or

$$\boldsymbol{z_t} = \begin{bmatrix} 1 & 0 & 0 & 0 \\ 0 & 1 & 0 & 0 \end{bmatrix} \begin{bmatrix} \omega_t \\ i_t \\ k_{T,t} \\ b_t \end{bmatrix} + \boldsymbol{v}_t \tag{5}$$

where u_t stands for the input operation parameter which is the voltage V at the current time t. In the equations, $\boldsymbol{w_t}$ and $\boldsymbol{v_t}$ represent the process and measurement noise which are assumed to be the Gaussian distribution with zero mean and the covariances Q and R, respectively.

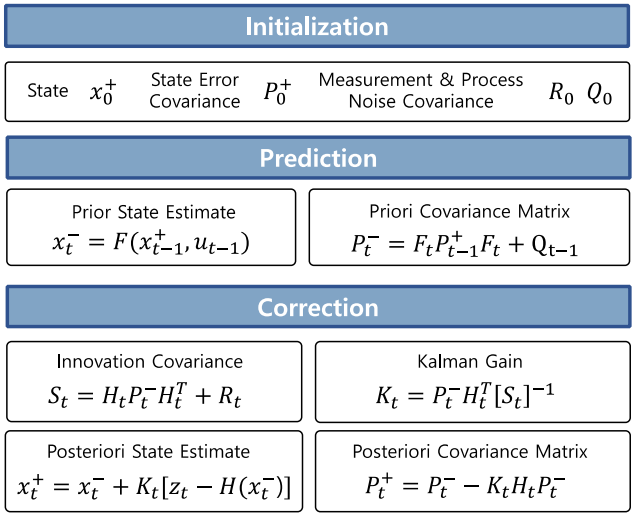

Fig. 4. Process of Extend Kalman Filter.

The overall process of the EKF is illustrated in Fig. 4, which is decomposed into two steps: prediction and correction. In the prediction step, the prior prediction of the state

variable x_t^- at current time t (denoted by "$-$") is made from those at the previous time $t-1$ using the state model under a given input u. The error covariance P_t^- is also predicted where F_t is a matrix form described in Eq. (4). Then in the correction step, the posterior update (denoted by $''+''$) is made by the measurement model, which leads to the corrected estimation of state variables by the measured data. Note that K_t and S_t denote the Kalman gain and covariance of the innovation term $z_t - H(x_t^-)$ respectively. The posterior update of state variables x_t^+ and error covariance P_t^+ become the initial estimate in the next time step $t+1$ and the two steps are recursively performed to converge to the true values.

In the EKF, it is common that the initial values of process and measurement noise covariance are assumed by arbitrary values and kept as a constant during the process. Assigning improper values, however, adversely affect and degrade the EKF's performance greatly. To overcome this, an Adaptive EKF (AEKF) by (Akhlaghi et al., 2018) is employed in this study to adaptively estimate the covariance matrixes at each step of the EKF. Let us define the difference between the measurement and the prediction as innovation (ρ), and the difference between the measurement and the correction as residual (ε).

$$\rho_t = z_t - H(x_t^-) \tag{6}$$

$$\varepsilon_t = z_t - H(x_t^+) \tag{7}$$

Then the measurement and process noise covariances are recursively estimated as follows.

$$R_t = \alpha R_{t-1} + (1-\alpha)(\varepsilon_t \varepsilon_t^T + H_t P_t^- H_t^T) \tag{8}$$

$$Q_t = \alpha Q_{t-1} + (1-\alpha)(K_t \rho_t \rho_t^T K_t^T) \tag{9}$$

where α denotes a forgetting factor ranging in $(0,1)$ for adaptive estimation. Note that a larger α indicates more weights on previous estimates and incurs less fluctuation of the covariance and longer time delays to adapt with changes. In this paper, set $\alpha = 0.8$ for all the studies.

3.2. Motor system performance evaluation

In the evaluation of the motor system performance in the satellite, a characteristic curve is usually used, which is defined by the relation between the output torque ($T_{output} = J\dot{\omega}$) and the angular velocity (ω) during the pull-up range. A typical characteristic curve is shown in Fig. 5, which is given by the straight blue line. To ensure the minimum actuation performance of RW, the motor needs to generate at least 5 mN · m of output torque at $\omega^* = 314.16$ rad/s, i.e., the motor is considered failure when the curve falls below this point as shown in the figure. This is a design requirement for the STSAT-3 (Kim et al., 2010) mission where the satellite with an inertial moment of 18 kgm^2 need to maneuver 25° in 40 s. Under this context, the motor system performance is defined by P_{sys} as follows:

$$P_{sys} = J\dot{\omega}|_{\omega=\omega^*} \tag{10}$$

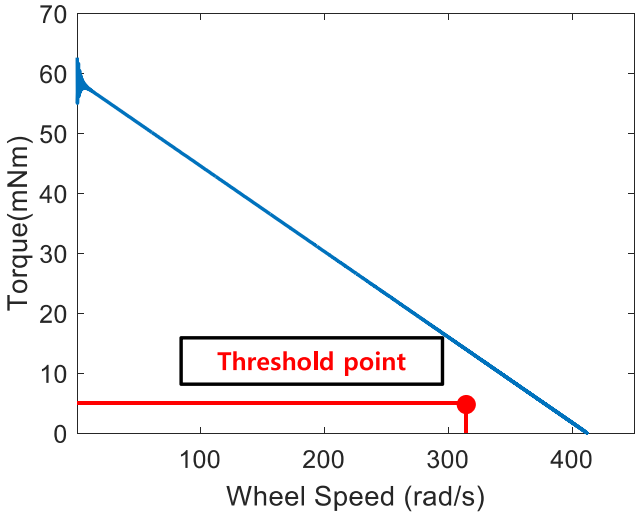

Fig. 5. SRB-361-1103 motor characteristic curve.

and the failure threshold point is given by 5 mN · m.

3.3. Off-line prognosis and monitoring

In the off-line monitoring and prognosis, the health parameters $\boldsymbol{h}$ estimated from the on-line diagnosis for each cycle are transferred, and monitored until the current cycle. The empirical degradation model is introduced to describe the health degradation over long-term cycles in a quantitative way, in which the model parameters are estimated using the accumulated health parameters. Particle Filter (PF) is used for this purpose, which is to recursively estimate the probability density function (pdf) of the long-term health state and model parameters in the form of particles (An et al., 2013; Orchard and Vachtsevanos, 2009). PF has advantages in managing the uncertainty in prediction and estimating the pdf in a nonlinear system with non-Gaussian noise. The future trend is then predicted by extrapolating each particle to the future cycles. As in the EKF, standard PF also consists of state transition function f and measurement function h as follows:

$$x_k = f(x_{k-1}, \beta_k) \tag{11}$$

$$z_k = h(x_k, n_k) \tag{12}$$

where k is the cycle step index, x_k is the estimated health state, β_k is the degradation model parameter, z_k is the measurement data which is in this case the health parameter values obtained by the on-line estimation, and n_k is the measurement noise. It is noted that while the two functions F and H in Eqs. (4), (5) are the state and measurement models for the motor dynamics in EKF formulation, the functions f and h here represent those for the empirical degradation model. In order to present the degradation in this study, an empirical based exponential function (Barbieri et al., 2015; Bejaoui et al., 2020; Yang et al., 2021) is employed for the function f:

$$f(x_{k-1}, \beta_k) = exp(\beta_k dt) x_{k-1} \tag{13}$$

The measurement noise is assumed by the Gaussian pdf, i.e., $n_k \sim N(0, \sigma_k)$, where σ_k is the unknown standard deviation. Consequently, the unknown parameters to be estimated are $\theta = [x, \beta, \sigma]^T$. It should be emphasized that the health parameters are estimated by the motor dynamic model using the AEKF at the on-line stage, whereas its trend over long-term cycles are estimated by the degradation model using the PF at the off-line stage. Once the degradation model is estimated up to the current cycle, it is used to predict the RUL for the future.

In the off-line prognosis, it is often the case that the degradation trend tends to accelerate after a certain cycle or initial fault. In order to account for this in the PF process, Shifting Kernel Particle Filter (SKPF) is used, which adds the capability to detect whether the current cycle deviates from the normal condition (Kim et al., 2020). To this end, the SKPF calculates the likelihood L, followed by calculating the decision function d_k:

$$L\left(z_k|x_k^i, \beta_k^i, \sigma_k^i\right) = \frac{1}{\sqrt{2\pi}\sigma_k^i} exp\left[-\frac{1}{2}\left(\frac{z_k - x_k^i\left(\beta_k^i\right\}}{\sigma_k^i}\right)^2\right] \quad (14)$$

$$d_k = -ln\left(\frac{1}{N}\sum_{i=1}^{N} L(z_k|x_k^i, \beta_k^i, \sigma_k^i)\right) \quad (15)$$

When the observed degradation is close to the normal condition, the likelihood tends to be high, resulting in the negative value, and the degradation is not monitored. On the other hand, if the state degrades in a different fashion, e.g., deviates from the normal, the likelihood becomes lower, which leads to the value toward the positive value. By monitoring this over cycles and examining if the decision function reaches the positive value, the anomaly point is identified. Once detected, the SKPF shifts the kernel function used in the resampling step of PF and adapt to the new degradation trend.

4. Result

4.1. Health parameter estimation by AEKF

In this section, the result of health parameter estimation at each cycle using the AEKF is addressed. To apply the AEKF, the initial values are necessary, which are given as $\boldsymbol{x}_0 = \left[0, 0, 0.054, 10^{-5}\right]^T$ based on the motor specification, in which the first two are the state variable $[\omega, i]^T$ and the remaining are the health parameters $[k_T, b]^T$. The initial process and measurement noise covariances are assumed arbitrary as $Q = [10^{-5}0; 010^{-5}]$ and $R = [20; 00.1]$ respectively. Then after performing the AEKF, estimated heath parameters in a cycle at the early stage (normal condition) are given in Fig. 6, where the red and green line represent the mean and 95 % confidence intervals, respectively. The value at the end of the time is then used as the health value of the cycle.

The ALT test has ended at 658 and 600 cycles for cold and hot conditions respectively. The resulting health parameter estimates made for the whole cycles are plotted in Fig. 7 for both conditions. Among the results, the degradation of the friction coefficient (b) in cold condition is noticeable, while the others do not change much. Therefore, test data under cold condition is used in this study to verify the proposed methodology. The bearing degradation is found dominant in this test and responsible for the motor performance degradation. This conforms to the literature that have indicated the bearing as the most frequent failure mode in the RW motor (Jin et al., 2013; Wang et al., 2016).

4.2. Motor system performance

The characteristic curves obtained from the on-line diagnosis in each cycle are drawn in the Fig. 8(a) where x-axis is the angular velocity and y-axis is the output torque. The graph shows that the curve constantly decreases in its slope as the cycle proceeds and approaches the threshold point. Since the motor system performance is defined by the torque at $\omega^* = 314.14$ rad/s, they are given by the points in Fig. 8(b) in which the green dashed line is the threshold. Even though the test has lasted over 3 years with 658 cycles, the results indicate that the motor did not reach the final failure yet.

4.3. Off-line prognosis by SKPF

Once the health parameters are estimated for each cycle, they are transferred to the off-line prognosis stage. Using the data up to 658 cycles, the degradation models of each health parameter are estimated, and their future is predicted using the SKPF. The prognosis results for both health parameters are shown in Fig. 9(a) and (c). The blue dots and triangular marks represent the estimated health values and the detected anomaly points by the decision function. The red dashed and solid lines represent the median and predictive interval (PI) in the future. The Fig. 9(b) and (d) represent the trace of the anomaly decision function. The blue line with circle is the decision function value and red dotted line is the anomaly threshold set by the user. From the result of parameter b as shown in Fig. 9(c), it is clear that the SKPF successfully detects the initial point of the degradation trend change after 500 cycles. There are few anomalies detected before 500 cycles due to sudden abnormal measurements during normal conditions. This occurs frequently in real applications, but the estimation trend does not change because the following data stays within the normal conditions. Meanwhile, when the degradation pattern changes after 500 cycles, the SKPF algorithm successfully adapts to the new degradation trend. The trace of decision function shows that d_k significantly increases and exceeds the threshold when the estimated

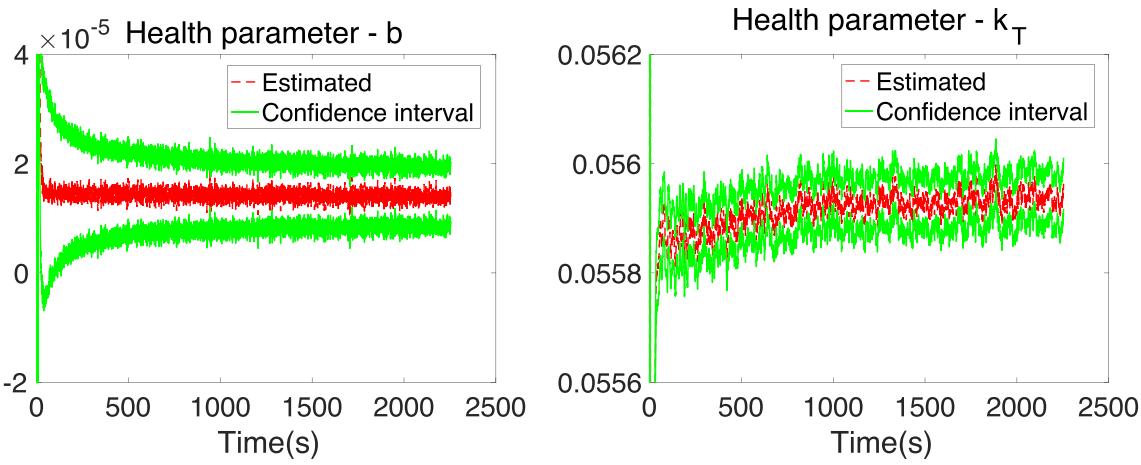

Fig. 6. Estimated health (k_T and b) in each cycle.

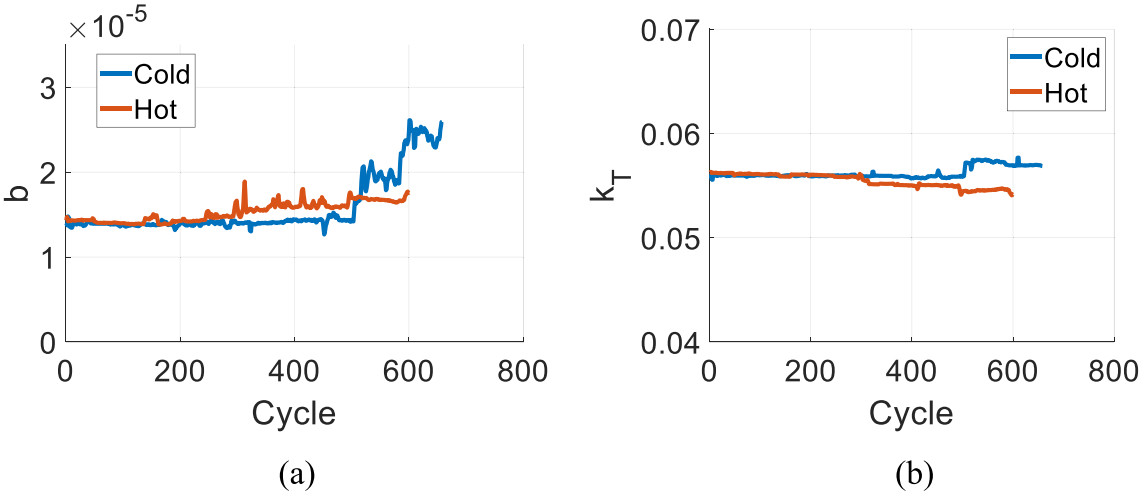

Fig. 7. Estimated health state (a) b and (b) k_T over cycles under cold and hot condition.

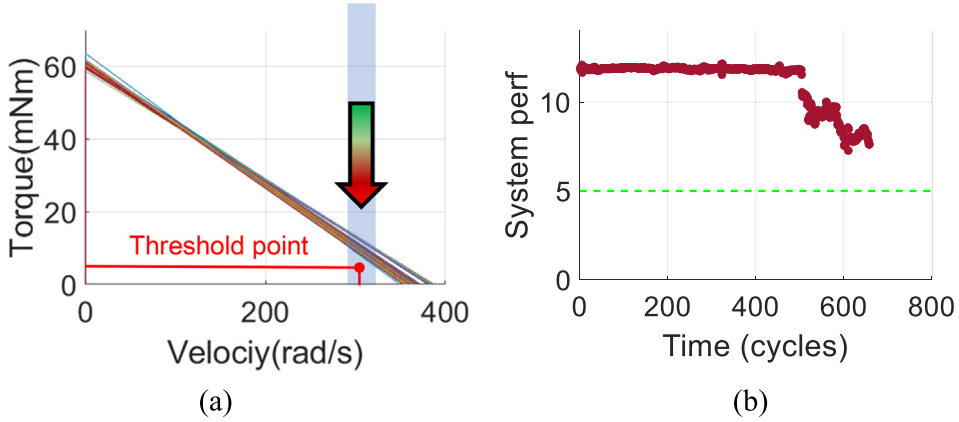

Fig. 8. (a) Characteristic curve and (b) system performance data of cold condition test.

state becomes incoherent with the observed data. After the algorithm adapts to the new degradation curve, it decreases back to the below threshold.

Once the health parameters are predicted at the future cycles, they are transferred up to the on-line stage. Then the health parameters are used in the state model to predict

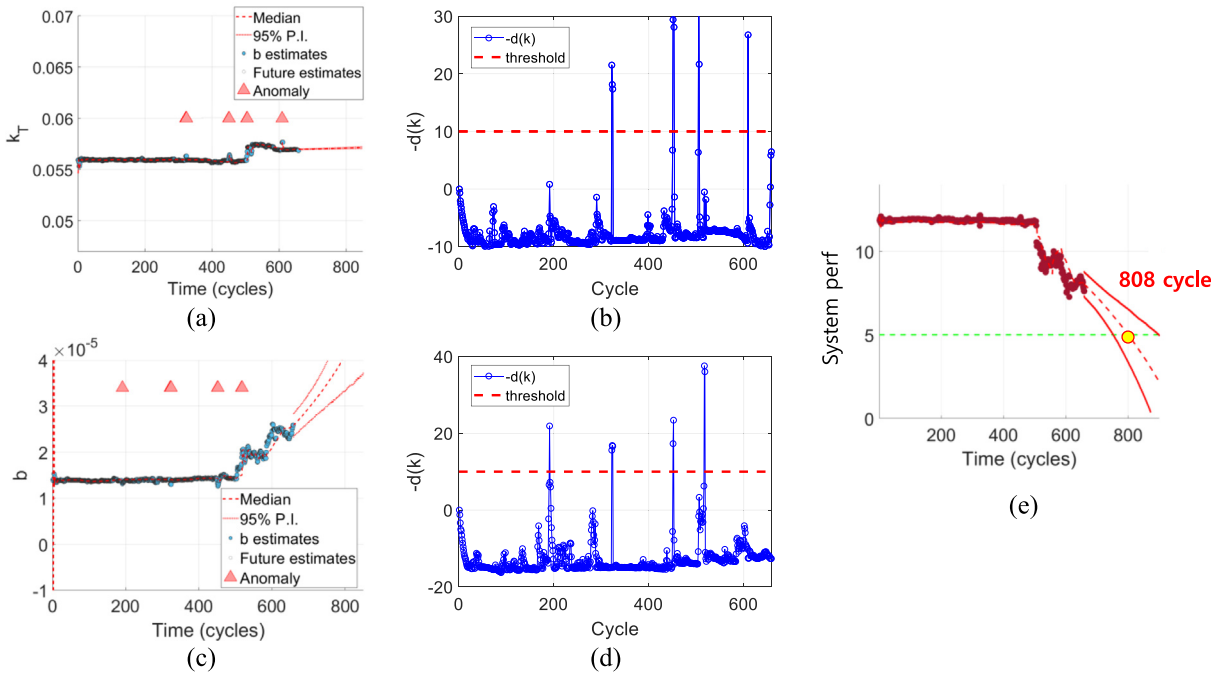

Fig. 9. (a) Prediction of parameter $\boldsymbol{k_T}$ by SKPF algorithm and (b) corresponding decision function (c) prediction of parameter $\boldsymbol{b}$ by SKPF algorithm and (d) corresponding decision function (e) prediction of system performance based on the health parameters.

the system performance. Then they are transferred down to the off-line stage. The results are given in the Fig. 9(e) with the median and 95 % PI. With the system threshold given by green dotted line, the EOL cycle for the system is predicted at 808 cycles, and the RUL being 150 cycles. It is emphasized again that the reason to predict RUL at 658 cycles is because the test has ended at this cycle. In order to validate this prediction, it is necessary to continue the test further to 808 cycles, and check whether it reaches the threshold line. This was however not implemented due to the limited cost and time. Instead, the validity of the prediction was confirmed by numerical simulation of the similar motor in the previous study by the authors (Kim et al., 2021).

5. Application of the framework to the RW motor in space

In the previous sections, the prognosis framework for the RW motor was implemented by the ALT data conducted on the ground. This section presents the feasibility of the proposed framework in the space. While a single cycle in the ALT consists of signals under pull-up and constant speeds as shown in Fig. 2, it is a little different in the space application. As shown in Fig. 1, the RW motor rotates in a pseudo-periodicity condition to provide consistent angular momentum to help stabilize the satellite from external torques such as low earth orbit aerodynamic forces, solar radiation pressure and etc. Based on the recent study on actual satellite telemetry (Zhang et al., 2021), telemetry signal tends to repeat periodic condition with some variability between time intervals due to space environment, interference and noise. Nevertheless, it is possible to use the measured data to estimate the health parameters in the motor dynamics model, and the same process applies to predict the RUL of the motor.

The steps are summarized in Table 3 and explained as follows. First, collect the motor operation data: motor current and velocity, for a cycle where the motor activates the RW for attitude control in space. In this study, virtual data of the speed and current are generated using the dynamic model by changing the input voltage according to the operating conditions (Zhang et al., 2021), and adding Gaussian white noise to express the measurement environment. The signals of input voltage and output speed and current are shown in Fig. 10. Second, conduct on-line diagnosis (estimation) using the data via AEKF to assess the current health parameters in the motor, which are b and k_T. The estimation results using virtual data are presented in Fig. 11 and health parameters are successfully estimated toward true value which root-mean square error (RMSE) for b and k_T are 0.015 and 0.017, respectively. If other components are presumed to degrade and affect the system performance as well, corresponding parameter should be identified in the model (1). Third, evaluate corresponding motor system performance under the current condition, which is defined by the output torque at $\omega^* = 314.16$ rad/s in the characteristic curve. Fourth, use the accumulated health parameters obtained at on-line diagnosis to estimate the off-line parameters in the degradation model by using the SKPF. Then their future behav-

Table 3
Steps for space application.

Application to space environment	
1. Motor operation data collection for a cycle with period	Virtual data in Fig. 10
2. Health estimation using the data via AEKF to assess the current health states of components	Estimation result in Fig. 11
3. Evaluate corresponding motor system performance based on the characteristic curve	Characteristic curve as shown in Fig. 8(a)
4. Using health data h_(0:k) up to the current cycle, predict their future behavior via SKPF	Prediction as shown in Fig. 9(a) & (c)
5. Transfer the predicted h to online estimation and obtain the system performance in the future for system RUL	System performance as shown in Fig. 9(e)

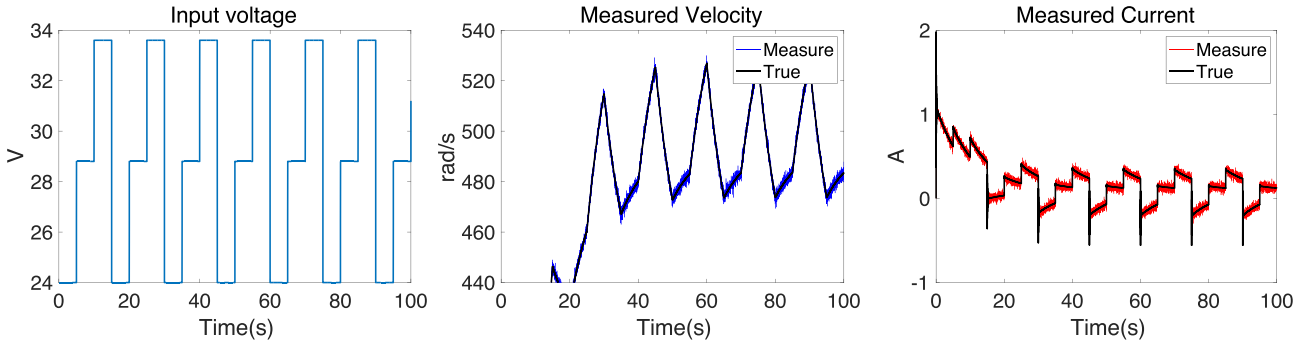

Fig. 10. Virtual data considering pseudo-periodicity and noise.

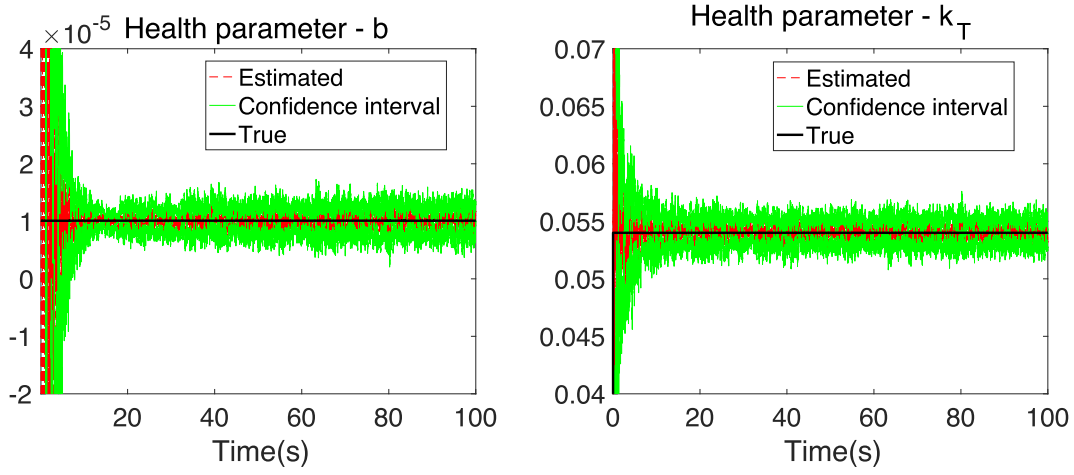

Fig. 11. Health parameter estimation result.

iors are predicted via extrapolating the degradation model. Finally, apply the health parameters in the on-line prediction to obtain the system performance in the future. Then the RUL can be calculated against its threshold. Using the predicted result, the operation engineer can make appropriate decision early before its failure such as shifting the mission to another satellite, plan to launch a new one, and so on.

6. Conclusions

In this research, the authors have proposed a PHM framework for the satellite RW motor not only to guarantee its safety and reliability, but also to aid decision making for the further operating schedule. The main contribution can be summarized as follows. First, the authors have conducted long-term ALT of RW over 3 years under harsh temperature conditions to evaluate the performance of the proposed method. Then, the future trend of the components health is predicted using the results of on-line diagnosis, and the system health degradation is predicted as well. By imposing the failure threshold for the system, the RUL of the motor is obtained while it is in operation. The uniqueness of the study is that it proposes advanced prognostics framework, integrating the component-level prognosis into the system. Although it is demonstrated for the dataset from ALT on the ground, the framework applies the same in the satellite operation in space, and provides effective means to aid decision making for the next action as early as possible using the predicted RUL.

However, further study is needed to enhance the practicality of the study. The experiment until failure data will be acquired to validate the capability of the proposed method more robustly. Also, the degradation difference between accelerated test and real operating conditions needs to be considered to effectively implement in the real satellite monitoring system. Moreover, other available models in the literature will be considered to have a more comprehensive sub-division of the components and various prognosis algorithms to effectively implement the framework in the real system.

Declaration of Competing Interest

The authors declare that they have no known competing financial interests or personal relationships that could have appeared to influence the work reported in this paper.

Acknowledgement

This research was supported by the National Research Foundation of Korea (NRF) grant funded by the Korean government (MSIT) (No. 2020R1A4A4079904) and the MOTIE (Ministry of Trade, Industry, and Energy) in Korea, under the Fostering Global Talents for Innovative Growth Program (P0017307) supervised by the Korea Institute for Advancement of Technology (KIAT).

References

Abd-Elhay, A.E.R., Murtada, W.A., Youssef, M.I., 2022. A Reliable deep learning approach for time-varying faults identification: spacecraft reaction wheel case study. IEEE Access 10, 75495–75512.

Aghalari, A., Shahravi, M., 2017. Nonlinear electromechanical modelling and dynamical behavior analysis of a satellite reaction wheel. Acta Astronaut. 141, 143–157.

Akhlaghi, S., Zhou, N., Huang, Z., 2018. Adaptive adjustment of noise covariance in Kalman filter for dynamic state estimation. In: IEEE Power and Energy Society General Meeting 2018-Janua, 1–5.

An, D., Choi, J.H., Kim, N.H., 2013. Prognostics 101: A tutorial for particle filter-based prognostics algorithm using Matlab. Reliab. Eng. Syst. Saf. 115, 161–169.

Barbieri, F., Hines, J.W., Sharp, M., Venturini, M., 2015. Sensor-based degradation prediction and prognostics for remaining useful life estimation: Validation on experimental data of electric motors. Int. J. Progn. Health Manag. 6, 1–20.

Bavdekar, V.A., Deshpande, A.P., Patwardhan, S.C., 2011. Identification of process and measurement noise covariance for state and parameter estimation using extended Kalman filter. J. Process Control 21, 585–601.

Bejaoui, I., Bruneo, D., Xibilia, M.G., 2020. A data-driven prognostics technique and RUL prediction of rotating machines using an exponential degradation model. In: 7th International Conference on Control, Decision and Information Technologies, CoDIT 2020, pp. 703–708.

Cao, M., Zhang, T., Yu, B., Liu, Y., 2019. A method for interval prediction of satellite battery state of health based on sample entropy. IEEE Access 7, 141549–141561.

Hu, D., Sarosh, A., Dong, Y.F., 2012. A novel KFCM based fault diagnosis method for unknown faults in satellite reaction wheels. ISA Trans. 51, 309–316.

Ji, X.Y., Li, Y.Z., Liu, G.Q., Wang, J., Xiang, S.H., Yang, X.N., Bi, Y.Q., 2019. A brief review of ground and flight failures of Chinese spacecraft. Prog. Aerosp. Sci. 107, 19–29.

Jin, G., Matthews, D., Fan, Y., Liu, Q., 2013. Physics of failure-based degradation modeling and lifetime prediction of the momentum wheel in a dynamic covariate environment. Eng. Fail. Anal. 28, 222–240.

Jun, M., Smith, K., Wood, E., Smart, M.C., 2012. Battery capacity estimation of low-earth orbit satellite application. Int. J. Progn. Health Manag. 3, 1–9.

Kim, S., Kim, N.H., Choi, J.-H., 2021. A study towards appropriate architecture of system-level prognostics: physics-based and data-driven approaches (September 2021). IEEE Access PP, 1–1.

Kim, S., Park, H.J., Choi, J.-H., Kwon, D., 2020. A novel prognostics approach using shifting kernel particle filter of li-ion batteries under state changes. IEEE Trans. Ind. Electron. 0046, 1.

Kim, D.H., Yang, S., Cheon, D.I., Lee, S., Oh, H.S., 2010. Combined estimation method for inertia properties of STSAT-3. J. Mech. Sci. Technol. 24, 1737–1741.

Lee, K.H., Lim, S.M., Cho, D.H., Kim, H.D., 2020. Development of fault detection and identification algorithm using deep learning for nanosatellite attitude control system. Int. J. Aeronaut. Space Sci. 21, 576–585.

Liu, D., Wang, H., Peng, Y., Xie, W., Liao, H., 2013. Satellite lithium-ion battery remaining cycle life prediction with novel indirect health indicator extraction. Energies (Basel) 6, 3654–3668.

Muthusamy, V., Kumar, K.D., 2021. A novel data-driven method for fault detection and isolation of control moment gyroscopes onboard satellites. Acta Astronaut. 180, 604–621.

Muthusamy, V., Kumar, K.D., 2022. Failure prognosis and remaining useful life prediction of control moment gyroscopes onboard satellites. Adv. Space Res. 69, 718–726.

Nozari, H.A., Castaldi, P., Banadaki, H.D., Simani, S., 2019. Novel non-model-based fault detection and isolation of satellite reaction wheels based on a mixed-learning fusion framework. In: IFAC-PapersOnLine. Elsevier B.V., pp. 194–199.

Orchard, M.E., Vachtsevanos, G.J., 2009. A particle-filtering approach for on-line fault diagnosis and failure prognosis. Trans. Inst. Meas. Control 31, 221–246.

Rahimi, A., Kumar, K.D., Alighanbari, H., 2017. Fault estimation of satellite reaction wheels using covariance based adaptive unscented Kalman filter. Acta Astronaut. 134, 159–169.

Rahimi, A., Kumar, K.D., Alighanbari, H., 2020a. Fault isolation of reaction wheels for satellite attitude control. IEEE Trans. Aerosp. Electron. Syst. 56, 610–629.

Rahimi, A., Kumar, K.D., Alighanbari, H., 2020b. Failure prognosis for satellite reaction wheels using Kalman filter and particle filter. J. Guid. Control Dynam. 43, 585–588.

Rahimi, A., Saadat, A., 2020. Fault isolation of reaction wheels onboard three-axis controlled in-orbit satellite using ensemble machine learning. Aerospace Syst. 3, 119–126.

Singleton, R.K., Strangas, E.G., Aviyente, S., 2015. Extended kalman filtering for remaining-useful-life estimation of bearings. IEEE Trans. Ind. Electron. 62, 1781–1790.

Song, Y., Liu, D., Yang, C., Peng, Y., 2017. Data-driven hybrid remaining useful life estimation approach for spacecraft lithium-ion battery. Microelectron. Reliab. 75, 142–153.

Tudoroiu, N., Sobhani-Tehrani, E., Khorasani, K., 2006. Interactive bank of unscented Kalman filters for fault detection and isolation in reaction wheel actuators of satellite attitude control system. In: IECON Proceedings (Industrial Electronics Conference), pp. 264–269.

Wang, Y., Masoud, N., Khojandi, A., 2021. Real-time sensor anomaly detection and recovery in connected automated vehicle sensors. IEEE Trans. Intell. Transp. Syst. 22, 1411–1421.

Wang, J., Zheng, H., Li, Q., Wu, H., Zhou, B., 2016. Prognostic for on-orbit satellite momentum wheel based on the similitude method. Proceedings of 2015 Prognostics and System Health Management Conference, PHM.

Yang, F., Habibullah, M.S., Shen, Y., 2021. Remaining useful life prediction of induction motors using nonlinear degradation of health index. Mech. Syst. Sig. Process. 148, 107183.
Zhang, Y., Jia, X., Guo, B., 2018. Bayesian framework for satellite rechargeable lithium battery synthesizing bivariate degradation and lifetime data. J. Cent. South Univ. 25, 418–431.
Zhang, X., Wang, Z., Ma, J., Li, S., Suo, M., 2021. State-of-health prediction for reaction wheel of on-orbit satellite based on fourier broad learning system. IEEE Access 9, 125691–125705.
Zhou, J., Knedlik, S., Loffeld, O., 2010. INS/GPS Tightly-coupled integration using adaptive unscented particle filter. J. Navig. 63, 491–511.